Weak M(II)-Azide-4,4′-Bipy Ferromagnets Based on Unusual Diamondoid (M = Mn) and 2D Arrays (M = Co, Ni)

Susana Martín,[†] M. Gotzone Barandika,[†] Luis Lezama,[‡] J. Luis Pizarro,[§] Zurine E. Serna,[‡] J. Ignacio Ruiz de Larramendi,[†] M. Isabel Arriortua,[§] Teófilo Rojo,[‡] and Roberto Cortés*[,†]

Departamento de Química Inorgánica, Universidad del País Vasco, Aptdo. 450, E-01080 Vitoria, Spain and Aptdo. 644, E-48080 Bilbao, Spain, and Departamento de Mineralogía-Petrología, Universidad del País Vasco, Aptdo. 644, E-48080 Bilbao, Spain

Received September 21, 2000

Four compounds of general formula $[M(4,4'bipy)(N_3)_2]_n$ (M = Mn (**1**), Zn (**2**), Co (**3**), Ni (**4**)) have been synthesized and magnetostructurally characterized by means of X-ray diffraction analysis, IR and ESR spectroscopies, and measurements of the magnetic susceptibility and magnetization. Compound **1** ($C_{10}H_8N_8Mn$) crystallizes in the tetragonal $P4_32_12$ space group, $Z = 4$, with $a = 8.229(2)$, $b = 8.229(2)$, and $c = 16.915(2)$ Å. It exhibits an acentric 3D structure where Mn(II) ions are linked through EE-azide groups resulting in a diamondoid network. The 4,4′bipy ligands are coordinated on the axial positions of the octahedral spheres reinforcing the intermetallic connections. Weak ferromagnetism arising from spin canting is observed for compound **1**. Compounds **2**, **3**, and **4** are proposed to be isomorphous and would consist of a 2D array where alternating EO + EE/EO + EE/EO + EO azide-chains are linked by 4,4′bipy ligands resulting in $\pi-\pi$ stacked pyridyl-columns. The azido ligand dispositions in compounds **3** and **4** make possible systems of type −AF−AF−F−, which would give rise to a topological ferromagnetic behavior.

Introduction

Over the last years, enormous efforts have been made in the synthesis of new coordination polymers of high dimensionality on the basis of concepts such as crystal engineering, molecular architectures, etc.[1] One of the points to be seriously considered for the preparation of these systems is the selection of the appropriate ligands, an aspect that is specially relevant if magnetic frameworks are desired.

The pseudohalide azide has been demonstrated to be not only an extremely versatile ligand but also an excellent magnetic coupler. Thus, a large number of azide-bridged systems from dimers to 3D-compounds has been synthesized and magneto-structurally characterized up to now.[2] Even if the number of 1D[3] and 2D[4] systems reported is remarkable (the dimensionality just referred to the links through azide groups), to our best knowledge, just two azide-bridged 3D magnetic systems have been reported so far:[5] $[Mn(py)_2(\mu_{1,3}-N_3)_2]_n$ (py = pyridine) and $[N(CH_3)_4]_n[Mn(\mu_{1,3}-N_3)_3]_n$. Both compounds exhibit several analogies such as the nature and octahedral coordination of the metallic cation and the *end-to-end* performance of the azide ligand.

The above-mentioned azide-bridged molecular architectures are specially interesting as they concern several coordination modes that provide a variety of magnetic couplings. In addition to the "usual" (1,3)-N_3 bridges (end-to-end, EE) associated with antiferromagnetic coupling and (1,1)-N_3 connections (end-on, EO) related with ferromagnetic exchange, other possibilities must also be taken into account. Thus, combined EO + EE links,[6] and alternating bridges[3a,b,d,7] have also been reported for the azide ligand. Obviously, the magnetic behavior is expected to reflect this potential in coordination performance.

* To whom correspondence should be addressed.
[†] Departamento de Química Inorgánica, Facultad de Farmacia.
[‡] Departamento de Química Inorgánica, Facultad de Ciencias.
[§] Departamento de Mineralogía-Petrología, Facultad de Ciencias.

(1) (a) Lehn, J. M. *Supramolecular Chemistry*; VCH: Weinheim, 1985; Chapter 9. (b) Robin, R.; Abrahms, B. F.; Barten, R. R.; Gable, R. W.; Huskiness, B. F.; Lieu, J. *Supramolecular Arquitecture*; American Chemical Society: Washington, DC, 1992; Chapter 9.
(2) Ribas, J.; Escuer, A.; Monfort, M.; Vicente, R.; Cortés, R.; Lezama, L.; Rojo, T. *Coord. Chem. Rev.* **1999**, 193−195, 1027.
(3) (a) Ribas, J.; Monfort, M.; Díaz, C.; Bastos, C.; Solans, X. *Inorg. Chem.* **1994**, *33*, 484. (b) Cortés, R.; Lezama, L.; Pizarro, J. L.; Arriortua, M. I.; Solans, X.; Rojo, T. *Angew. Chem., Int. Ed. Engl.* **1994**, *33*, 2488. (c) Ribas, J.; Monfort, M.; Kumar-Gosh, B.; Solans, X.; Font-Bardía, M. *J. Chem. Soc., Chem. Commun.* **1995**, 2375. (d) Ribas, J.; Monfort, M.; Resino, I.; Solans, X.; Rabu, P.; Maingot, F.; Drillon, M. *Angew. Chem., Int. Ed. Engl.* **1996**, *35*, 2520. (e) De Munno, G.; Poerio, T.; Viau, G.; Julve, M.; Lloret, F.; Journaux, Y.; Riviere, E. *Chem. Commun.* **1996**, 2587. (f) Cortés, R.; Drillon, M.; Solans, X.; Lezama, L.; Rojo, T. *Inorg. Chem.* **1997**, *36*, 677. (g) Viau, G.; Lombardi, M. G.; De Munno, G.; Julve, M.; Lloret, F.; Faus, J.; Caneschi, A.; Clemente-Juan, J. M. *J. Chem. Soc., Chem. Commun.* **1997**, 1195. (h) Borrás-Almenar, J. J.; Clemente-Juan, J. M.; Coronado, E.; Lloret, F. *Chem. Phys. Lett.* **1997**, *275*, 79. (i) Cortés, R.; Urtiaga, M. K.; Lezama, L.; Pizarro, J. L.; Arriortua, M. I.; Rojo, T. *Inorg. Chem.* **1997**, *36*, 5016. (j) Esposito, F.; Kamieniarz, G. *Phys. Rev. B* **1998**, *57*, 7431. (k) Escuer, A.; Font-Bardía, M.; Peñalba, E.; Solans, X.; Vicente, R. *Polyhedron* **1998**, *18*, 211. (l) Escuer, A.; Vicente, R.; Goher, M. A. S.; Mautner, F. A. *Inorg. Chem.* **1998**, *37*, 782. (m) Goher, M. A. S.; Mautner, F. A. *Polyhedron* **1998**, *17*, 1561. (n) Hernández, M. L.; Barandika, M. G.; Urtiaga, M. K.; Cortés, R.; Lezama, L.; Arriortua, M. I. *J. Chem. Soc., Dalton Trans.* **2000**, 79.
(4) (a) Escuer, A.; Vicente, R.; Goher, M. A. S.; Mautner, F. A. *Inorg. Chem.* **1995**, *34*, 5707. (b) Escuer, A.; Vicente, R.; Goher M. A. S.;. Mautner F. A. *Inorg. Chem.* **1996**, *35*, 6386. (c) Escuer, A.; Vicente, R.; Goher, M. A. S.; Mautner, F. A. *J. Chem. Soc., Dalton Trans.* **1997**, 4431. (d) Escuer, A.; Vicente, R.; Goher, M. A. S.; Mautner, F. A. *Inorg. Chem.* **1997**, *36*, 3440.
(5) (a) Goher, M. A. S.; Mautner, F. A.; *Croat. Chim. Acta* **1990**, *63*, 559. (b) Mautner, F. A.; Hanna, S.; Cortés, R.; Lezama, L.; Barandika, M. G.; Rojo, T. *Inorg. Chem.* **1999**, *38*, 4647.
(6) (a) Mautner, F. A.; Goher, M. A. S. *Polyhedron* **1995**, *14*, 1809. (b) Escuer, A.; Vicente, R.; El Fallah, M. S.; Goher, M. A. S.; Mautner, F. A. *Inorg. Chem.* **1998**, *37*, 4466.

10.1021/ic001067q CCC: $20.00
Published on Web 07/13/2001

The strategy for the preparation of coordination polymers has been systematically raised by enhancing the self-assembly of structural units of lower dimensionality through covalent bonds. The latter can be carried out by using rigid, rodlike organic building blocks such as the bifunctional 4,4′-bipyridine (4,4′bipy) as illustrated by the high number of polymeric compounds bridged by this ligand.[8]

Taking into account the above-mentioned aspects, this work was focused on the preparation of M(II)−$(N_3)_2$-4,4′bipy extended structures. The results concern the synthesis and magnetostructural characterization of four compounds exhibiting the general formula $[M(4,4'bipy)(N_3)_2]_n$ (M = Mn(**1**),[9] Zn(**2**), Co(**3**), Ni(**4**)). Compound **1** exhibits an acentric 3D structure based on a diamondoid azide-linked network. Compounds **2**, **3**, and **4** are proposed to be isomorphous and would consist of a 2D array with $\pi-\pi$ stacked columns of pyridyl rings where alternating EO + EE/EO + EE/EO + EO bridges are present.

Experimental Section

Materials. Manganese(II) nitrate (Aldrich), zinc(II) sulfate (Aldrich), cobalt(II) nitrate (Fluka), nickel(II) nitrate (Fluka), and sodium azide (Sigma) were purchased and used without further purification.

Caution! Azide metal complexes are potentially explosive. Only a small amount of material should be prepared, and it should be handled with caution.

Synthesis. Compound **1** was synthesized by slow addition of a methanolic solution of 4,4′bipy (0.080 g, 0.5 mmol) to an aqueous/methanolic solution containing $Mn(NO_3)_2 \cdot 4H_2O$ (0.144 g, 0.5 mmol) and NaN_3 (0.065 g, 1 mmol). The reaction was carried out under continuous stirring at 45 °C. The resulting solution was left to stand at room temperature. After four weeks, yellowish, prismatic, X-ray quality single crystals were obtained.

Compound **2** was synthesized by following the same procedure but using an aqueous solution of $Zn(SO_4) \cdot 7H_2O$ (0.144 g, 0.5 mmol) and NaN_3 (0.065 g, 1 mmol). In this case a white precipitate was immediately formed. For compounds **3** and **4**, the procedure used for **2** was followed with $Co(NO_3)_2 \cdot 6H_2O$ (0.146 g, 0.5 mmol) and $Ni(NO_3)_2 \cdot 6H_2O$ (0.146 g, 0.5 mmol). As for **2**, brownish (**3**) and green (**4**) precipitates were immediately formed. Further attempts to recrystallize these precipitates gave rise to poor quality single crystals.

Elemental analysis and ICP results were in good agreement with the $MC_{10}N_8H_8$ stoichiometry for all the compounds. Yield: 67%, 81%, 86% and 82% for **1**−**4**, respectively. Anal. found (calc.) %: Mn, 19.21 (18.61); N, 36.50 (37.96), C 40.47 (40.69); H 2.88 (2.73) for **1**: Zn, 21.20 (21.39); N, 37.03 (36.67), C 38.96 (39.3); H 2.81 (2.64) for **2**: Co, 20.50 (19.70); N, 36.91 (37.46), C 39.95 (40.15); H 2.83 (2.70) for **3**: Ni, 20.50 (19.63); N, 36.52 (37.49), C 40.02 (40.18); H 2.75 (2.70) for **4**.

Table 1. Crystal Data and Structure Refinement for Compound **1**

empirical formula	$MnC_{10}N_8H_8$	Z	4
fw	295.18	ρ_{calc}, g cm^{-3}	1.712
space group	$P\,4_3\,2_1\,2$ (No. 96)	ρ_{obs}, g cm^{-3}	1.65(4)
a, Å	8.229(2)	μ, mm^{-1}	1.15
b, Å	8.229(2)	T, K	293
c, Å	16.915(2)	λ, Å	0.71070
V, Å^3	1145.4(6)	R1[a] [$I > 2\sigma(I)$]	0.040
		wR2[b]	0.087

[a] $R1 = [\sum||F_o| - |F_c||/\sum|F_o|]$. [b] $wR2 = [\sum[w(F_o^2-F_c^2)^2]/\sum[w(F_o^2)^2]]^{1/2}$, where $w = 1/\sigma^2(|F_o|)$.

Physical Measurements. Microanalyses were performed with a LECO CHNS-932 analyzer. Analytical measurements were carried out in an ARL 3410 + ICP with a Minitorch equipment. IR spectroscopy was performed on a Nicolet 520 FTIR spectrophotometer in the 400−4000 cm^{-1} region. ESR spectroscopy was performed on powdered samples at X frequency, with a Bruker ESR 300 spectrometer, equipped with a standard OXFORD low-temperature device, calibrated by the NMR probe for the magnetic field, the frequency being measured by using a Hewlett-Packard 5352B microwave frequency computer. Magnetic susceptibilities and magnetization of powdered samples were carried out in the temperature range 1.8−300 K at values of the magnetic field up to 70 000 G, using a Quantum Design Squid magnetometer, equipped with a helium continuous-flow cryostat. The experimental susceptibilities were corrected for the diamagnetism of the constituent atoms (Pascal tables). Heat-capacity measurements were performed on a Quantum Design microcalorimeter between 2 and 100 K using powdered samples.

X-ray Crystallography. Preliminary communications about the crystal structure of **1** were published by Shen et al. ($P4_12_12$ space group), Han et al., and ourselves,[9] so we will describe here the mean and new data obtained for this compound. The structure has been solved in the $P4_32_12$ space group. Enraf-Nonius CAD-4 diffractometer with graphite-monochromated Mo Kα radiation (λ = 0.71073 Å). Corrections for Lorentz and polarization. Heavy-atoms Patterson methods using the program SHELXS86[10] and refined by a full-matrix least-squares procedure on F^2 using SHELXL93.[11] Non-hydrogen atomic scattering factors were taken from International Tables of X-ray Crystallography.[12] Crystallographic data and processing parameters for compound **1** are shown in Table 1.

X-ray powder diffraction data for compounds **2**, **3**, and **4** were collected on a PHILIPS X'PERT powder diffractometer with Cu Kα radiation in steps of 0.02° (2θ) over the 5−60° (2θ) angular range and a fixed-time counting of 4 s at 25 °C. The powder diffraction patterns of **3** and **4** show a low degree of crystallinity. The analysis of the diffraction data for all compounds was carried out using the FULLPROF[13] program, based on the Rietveld method.[14−15] For compound **2**, the coordinates of the crystal structure reported by Pan et al.[16] were used as starting structural model. A preliminary Rietveld refinement showed a high degree of preferred orientation due to the strong intensity of the (−2 0 0). This effect was corrected using the Martz function in the refinements. The parameters varied in the Rietveld analysis were the following: cell parameters, zero point, profile parameters (u, v, w, ETA), overall temperature factor, asymmetry, and preferred orientation parameters.

(7) (a) Tang, L.-F.; Zhang, L.; Li, L.-C.; Cheng, P.; Wang, Z.-H.; Wang, J.-T. *Inorg. Chem.* **1999**, *38*, 6326. (b) Abu-Youssef, M. A.; Escuer, A.; Gatteschi, D.; Goher, M. A. S.; Mautner, F. A.; Vicente, R. *Inorg. Chem.* **1999**, *38*, 5716. (c) Abu-Youssef, M.; Escuer, A.; Goher, M. A. S.; Mautner, F. A.; Vicente, R. *Eur. J. Inorg. Chem.* **1999**, 687. (d) Goher, M. A. S.; Al-Salem, N. A.; Mautner, F. A. *J. Coord. Chem.* **1998**, *44*, 119. (e) Youssef, M. A.; Escuer, A.; Goher, M. A. S.; Mautner, F. A.; Vicente, R. *J. Chem. Soc., Dalton Trans.* **2000**, 413.

(8) (a) Fujita, M.; Kwon, Y. J.; Washizu, S.; Ogura, K. *J. Am. Chem. Soc.* **1994**, *116*, 1151. (b) Kondo, M.; Yoshitomi, T.; Seki, K.; Matsuzaka, H.; Kitagawa, S.; *Angew. Chem., Int. Ed. Engl.* **1997**, *36*, 1725. (c) Lu, J.; Paliwala, T.; Lim, S. C.; Yu, C.; Niu, T.; Jacobson, A. J. *Inorg. Chem.* **1997**, *36*, 923. (d) Tong M. L.; Ye, B. H.; Cai, J. W.; Chen, X. M.; Ng, S. W. *Inorg. Chem.* **1998**, *37*, 2645. (e) Tong, M. L.; Chen, X. M.; Yu, X. L.; Mak, T. C. W. *J. Chem. Soc., Dalton Trans.* **1998**, 5. (f) Lu, J. Y.; Cabrera, B. R.; Wang, R.-J.; Li, J. *Inorg. Chem.* **1999**, *38*, 4608. (g) Lu, J. Y.; Lawandy, M. A.; Li, J.; Yuen, T.; Lin, C. L. *Inorg. Chem.* **1999**, *38*, 2695. (h) Zheng, L.-M.; Fang, X.; Lii, K.-H.; Song, H.-H.; Xin, X.-Q.; Fun, H.-K.; Chinnakali, K.; Razak, I. A. *J. Chem. Soc., Dalton Trans.* **1999**, 2311.

(9) (a) Shen, H. Y.; Liao, Z. H.; Yan, S. P.; Sun, B. W.; Yao, X. K.; Wang, H. G. *Chem. Lett.* **1998**, 469. (b) Cortés, R.; Martin, S.; Lezama, L.; Barandika, M. G.; Rojo, T.; Pizarro, J. L. *Proceedings of the XXXIII ICCC*; 1998; p 352. (c) Han, S.; Manson, J. L.; Kim, J.; Miller, J. S. *Inorg. Chem.* **2000**, *39*, 4182.

(10) Sheldrick, G. M. *SHELXS86. Program for the Solution of Crystal Structures*; University of Göttingen: Germany, 1985.

(11) Sheldrick, G. M. *SHELXL93. Program for the Refinement of Crystal Structures*; University of Göttingen: Germany, 1993.

(12) *International Tables for X-ray Crystallography*; Kynoch Press: Birmingham, UK, 1974; Vol. IV.

(13) Rodriguez Carvajal, J. *FULLPROF, Program Rietveld Pattern Matching Analysis of Powder Patterns*; 1997.

(14) Rietveld, H. M. *Acta Crystallogr.* **1967**, *12*, 151.

(15) Rietveld, H. M.; *J. Appl. Cryst.* **1969**, *6*, 65.

(16) Pan, L.; Zheng, N. W.; Wu, Y. G.; Huang, X. Y. *J. Coord, Chem,* **1999**, *47*, 551.

Table 2. Crystallographic Data for **2**, **3**, and **4**

compound	**2**	**3**	**4**
empirical formula	$Zn_3C_{30}N_{24}H_{24}$	$Co_3C_{30}N_{24}H_{24}$	$Ni_3C_{30}N_{24}H_{24}$
fw	916.82	897.48	896.75
crystal system	monoclinic	monoclinic	monoclinic
space group	*C*2/*m*	*C*2/*m*	*C*2/*m*
a, Å	19.988(3)	15.451(4)	14.945(6)
b, Å	11.432(3)	11.355(3)	11.060(4)
c, Å	11.252(3)	10.618(3)	10.375(4)
β, deg.	120.57(2)	115.42(2)	114.08(2)
Z	2	2	2
V, Å^3	1770.8(7)	1682.5(8)	1565(1)
T, K	273	273	273
λ, Å	1.5406,1.5444	1.5406,1.5444	1.5406,1.5444
R_b[a]	14.1		
R_p[b]	22.4	7.59	6.77
R_{wp}[c]	32.4	10.1	9.23
$N - P + C$	1816	1838	1839
X[d]	2.21	3.09	2.31

[a] $R_b = 100[\sum|I_{oi} - I_{ci}|]/\sum|I_o|$. [b] $R_p = 100[\sum|y_{oi} - y_{ci}|]/\sum|y_{oi}|$. [c] $R_{wp} = [M/\sum[w\ |y_{oi}|^2]]^{1/2}$. [d] $X = [M/N - P + C]^2$; R_p and R_{wp} values are background uncorrected. $M = \sum[w\ |y_{oi} - y_{ci}|^2]$; N = number of data; P = number of refined parameters; C = number of restrictions.

Due to the low crystallinity of the compounds **3** and **4**, the analysis of the powder diffraction data was performed using the *Profile Matching* option. The parameters varied were the following: cell parameters, zero point, profile parameters (u, v, w, ETA), and asymmetry parameters.

Crystallographic data and processing parameters for compounds **2**, **3**, and **4** are given in Table 2. The results obtained in the analysis of the powder diffraction data, together with that obtained by other techniques allow to propose compounds **2**, **3**, and **4** as isomorphous.

Results and Discussions

Crystal Structures. The structure of **1**, previously reported in communications by Shen et al. and ourselves,[9] consists of a 3D network in which Mn(II) cations are octahedrally coordinated to six N-atoms: four of them corresponding to single EE azides, on the equatorial positions, and two of them to 4,4′-bipy ligands, on the axial ones. The structure is rather complex as the six ligands connected to each metallic ion perform as intermetallic bridges. The pseudohalide ligands provide a tetrahedral topology around Mn(II) cations (Figure 1) resulting in an azide-linked diamondoid (Figure 2) network, where Mn−Mn distance is 5.938 Å. As observed in Figure 2, this diamondoid disposition accounts for the existence of adamantane-type cages where the 4,4′-bipy ligands are contained, bonded to the Mn(II) cations along the [1 1 0] and [1−1 0] directions (Mn−Mn distance through organic groups is 11.638 Å).

The structure of **2** was first reported by Pan et al.[16] (*C*2/*m*, $Z = 2$, $a = 16.00(2)$ Å, $b = 11.442(1)$ Å, $c = 11.272(1)$ Å, $\beta = 120.75(1)°$). Figure 3a shows the X-ray diffraction pattern analysis carried out on the powdered sample for **2** according to the crystallographic data in Table 2. Compound **2** consists of a 2D network (Figure 4) in which azide-brigded Zn(II)-chains are connected through 4,4′bipy ligands. Along the chains, the octahedrally coordinated metallic atoms are doubly bridged through azide groups (which occupy the equatorial positions) being the extension of the chains the result of the repetition of a sequence of three azide bridges along the [001] direction. Two consecutive EO + EE bridges are followed by a EO + EO one. The former bridges are related by a center of symmetry located on one of the metallic atoms. Thus, two types of octahedral spheres (A and B in Figure 4) can be found in this compound. The succession of 4,4′bipy planes at appropriate spacings (<3.8 Å) along the [010] direction provides the $\pi-\pi$ parallel stacking of pyridyl columns. These planes are packed along the *x* axis (Figure 4) which is the preferred orientation found for the powdered samples.

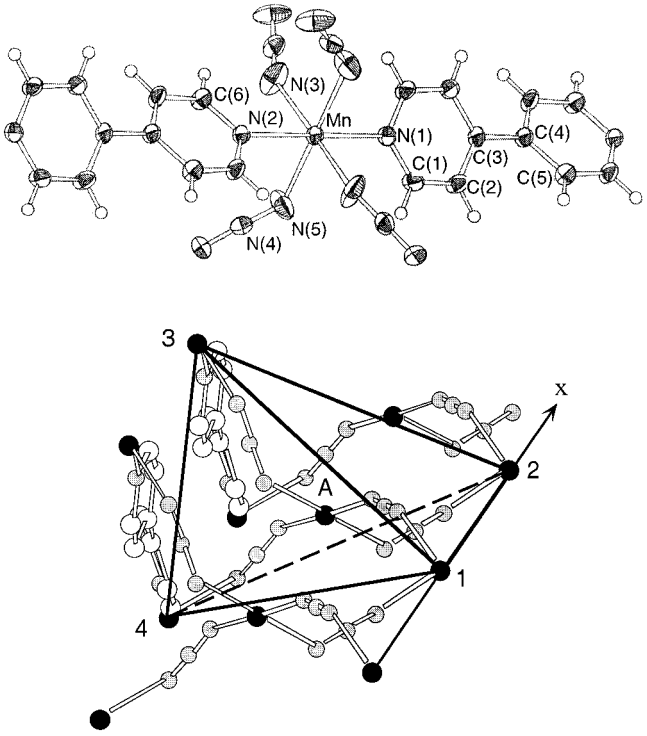

Figure 1. (a) Ortep view of the coordination polyhedron of **1**, with atom numbering scheme showing 50% probability ellipsoids. (b) Detail of the structure of **1** along the *x* direction showing the tetrahedral topology around Mn(II) ions.

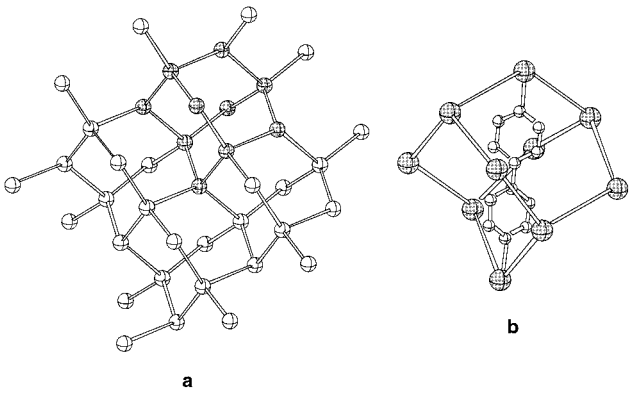

Figure 2. (a) Diamondoid network formed by the Mn(II) cations (an adamantane-cage is marked). (b) Detail of an adamantane-cage containing a coordinated 4,4′bipy group.

X-ray diffraction patterns for **3** and **4** were refined by using as initial values those corresponding to the cell parameters and space group of **2**. The experimental, calculated (according to the best fit parameters shown in Table 2), and difference patterns are shown in Figure 3b,c. These results may be indicative of isomosphism between **2**, **3**, and **4** compounds. Besides, taking into account that they have the same empirical formula and show very similar properties that will be developed herein after (IR, RSE, magnetic susceptibility), they can be proposed to have the same structural arrangement.

Comparison of compound **1** with **2**−**4** clearly shows the influence of the nature of the metallic cation on the final structural array of the complexes. Thus, as mentioned above, the only two 3D azide-bridged compounds reported so far[3] are also Mn(II)-compounds in which the cation is octahedrally

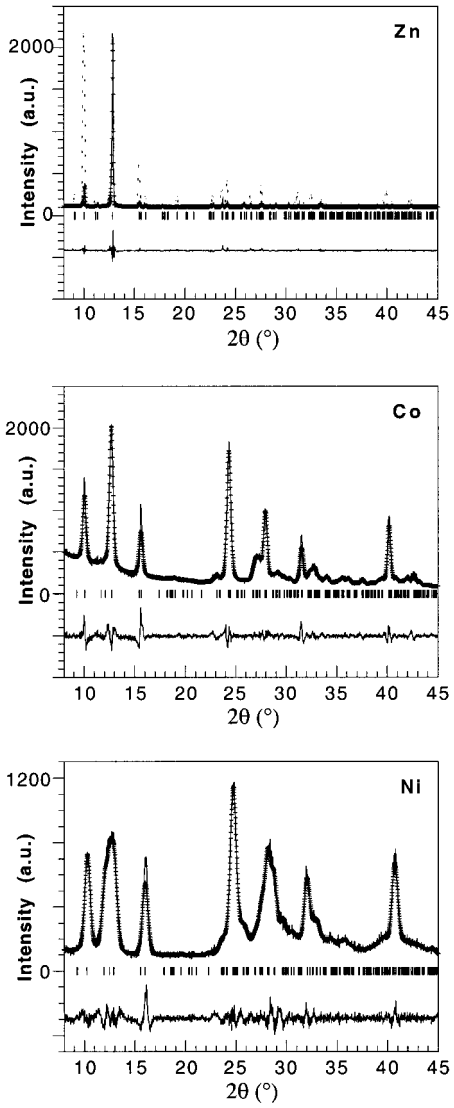

Figure 3. (a) Observed, calculated (preferred orientation), and difference X-ray diffraction pattern for **2**. The dotted line is the theoretical X-ray diffraction pattern. (b) and (c) Observed, calculated, and difference X-ray diffraction patterns for **3** and **4**, respectively.

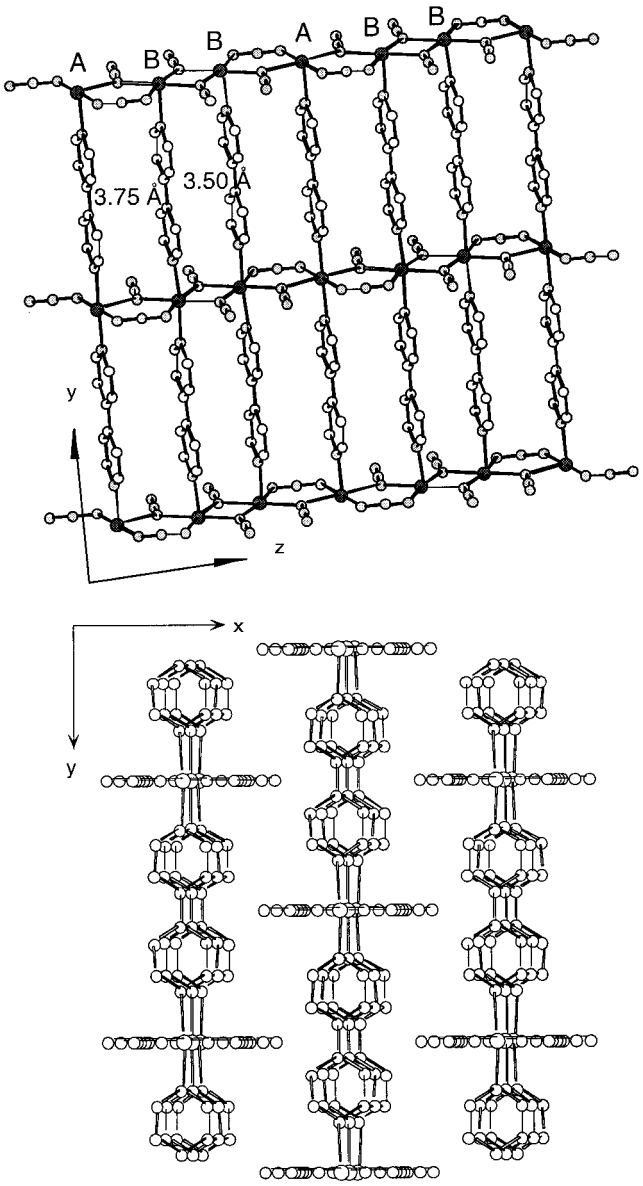

Figure 4. (a) View of the 2D array for **2**. (b) Packing of the layers along the *x* direction.

coordinated to four EE azide ligands. The singularity of **1** lies on the absence of a center of symmetry that is a requirement for many bulk properties of solid materials. In particular, the ferromagnetic performance of **1** will be discussed below under this condition.

Since the pioneering work of Ermer and Eling[17] on hydrogen-bonded networks of adamantane 1,3,5,7-tetracarboxylic acid and methanetetraacetic acid, diamondoid frameworks have been recognized as potential structural motifs for the construction of acentric solids. Considering that the typical strategy for the construction of this type of metal−organic coordination networks[18] implies the use of unsymmetrical spacers, compound **1** is also noticeable as an example of diamondoid array based on symmetrical bridging ligands.

In relation to the structures for **2**−**4,** it is worth mentioning that it exhibits an unusual combination of bridging types for the versatile azide ligand. As for **1**, this peculiar structural array will have significant consequences on the magnetic performance of **3** and **4** that will be analyzed in detail in the ESR and magnetic sections.

IR Spectroscopy. A summary of the most important IR bands corresponding to compounds **1**−**4** together with their tentative assignment[19] are contained in the Supporting Information.

The interest of the IR spectra of azide-bridged compounds is usually focused on the bands corresponding to this ambidentate ligand. Thus, the four spectra exhibit an intense absorption at about 2075 cm^{-1} which is associated with the asymmetric stretching mode of the azide ligand. The split of this band is indicative of the bridging performance of the azide in the four compounds. The fact that two coordination fashions are present in compounds **2**, **3**, and **4** can be also detected in the IR spectra, since the split of the bands is remarkably sharp. The presence of the symmetric vibration of the azide at about 1300 cm^{-1} (only detected in compounds **2**, **3**, and **4**) is indicative of the EO coordination of azide since this vibration mode is not usually active in EE azides. Finally, the four spectra exhibited the bands

(17) (a) Ermer, O.; Eling, A. *Angew. Chem., Int. Ed. Engl.* **1988**, *27*, 829. (b) Ermer, O. *J. Am. Chem. Soc.* **1988**, *110*, 3747.

(18) Evans, O. R.; Xiong, R.-G.; Wang, Z.; Wong G. K.; Lin, W. *Angew. Chem.* **1999**, *38*, 536.

(19) Nakamoto, K. *Infrared Spectra of Inorganic and Coordination Compounds*; John Wiley & Sons: New York, 1997.

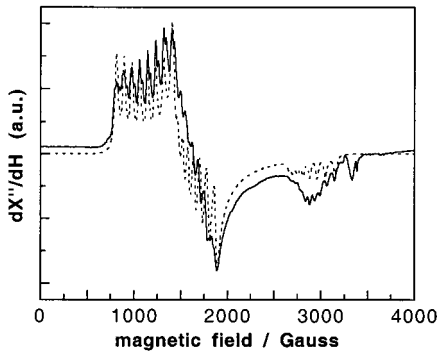

Figure 5. X-band powdered ESR spectrum for **2** doped with 0.1% Co; the discontinuous line is the calculated spectrum.

corresponding to the skeleton vibrations of the coordinated 4,4′-bipy. The IR spectra of compounds **2**−**4** are identical: that would be in agreement with the existence of the same structural disposition.

ESR Spectroscopy. The X-band room-temperature ESR spectrum for **1** is isotropic, centered at $g = 2.00$ and with a line width peak-to-peak of 50 G. With the aim of analyzing the environment of the M(II) cations in the 2D arrays for **2**−**4**, which are proposed to be isomorphous, we have doped the diamagnetic Zn(II) compound with Co(II) ion. ESR spectra were recorded at 4.2 K on powdered samples of compound **2** doped with several amounts of Co(II) (0.50, 0.3, 0.1, and 0.05%). The best resolution was found for the sample doped with 0.1% Co (Figure 5). As can be seen, the spectrum shows the strong anisotropy of the *g*-factor as well as the hyperfine coupling constant corresponding to the signals of two distinct Co(II) octahedral ions. According to the signals, these chromophores should be very similar, as corresponds to both MN_6 sites present in **2** (M_A and M_B, with statistical weights of $^1/_3$ and $^2/_3$, respectively) (Figure 5). This is in agreement with the proposed isomorphism.

Thus, the spectrum in Figure 5 can be described in terms of a spin doublet $S = {}^1/_2$ interacting with a single ^{59}Co nucleus ($I = {}^7/_2$). This effective spin doublet arises from the $^4T_1$ term through spin−orbit coupling and local distortion of the octahedral sites.[20] As observed, just the first signal is well resolved for the two chromophores. Therefore, average values of *g* and the hyperfine coupling constants have been determined for the last two signals. In this way, the observed *g*-values are $g_{1A} = 5.95$, $g_{1B} = 6.05$, $g_2 = 4.05$, and $g_3 = 2.30$. The sum of the three *g*-values for both Co_A and Co_B is close to 13, as proposed by Abragam and Pryce.[21] On the other hand, the hyperfine splitting parameters are $A_{1A} = 240 \times 10^{-4}$, $A_{1B} = 240 \times 10^{-4}$, $A_2 = 120 \times 10^{-4}$, and $A_3 = 75 \times 10^{-4}$ cm^{-1}. Figure 5 also shows the calculated spectrum for the Co_B chromophore that quite well reproduces the major characteristics of the observed signal.

The anisotropy for the *g* and *A* values would be explained by the distortion observed in the MN_6 octahedra. For the Zn(II) compound, Pan et al.[16] reported values of Zn−N distances from 2.14 to 2.27 Å, the first of them corresponding to a N-atom of the EO + EO bridge and the other one to the EE-bridged N-atom of the EO + EE bridge. Finally, a couple of weak signals at about 3400 G have been attributed to the presence of a very small amount of impurity.

Magnetic Properties. Measurements of the thermal variation of the magnetic susceptibility, χ_m, were carried out for compound **1** in the 2−300K range. Weak ferromagnetism for this compound was previously communicated.[9b−c] The thermal variation of χ_m^{-1} was fit by the Curie−Weiss expression, $\chi \propto (T - \theta)^{-1}$, with values of C_m and θ of 4.823 cm^{3}Kmol^{-1} and −79.8 K for $T > 100$ K, respectively, indicative of strong antiferromagnetic coupling between metal sites. The room temperature $\chi_m T$ value is 3.35 cm^{3}mol^{-1}K (Figure 6). This value is reduced from its value of 4.4 cm^{3}mol^{-1}K for uncoupled $S = {}^5/_2$ ions due to antiferromagnetic coupling, i.e., the large negative θ value. Below 300 K, the $\chi_m T$ value of **1** decreases gradually, reaching a minimum below 45 K attributed to long-range weak ferromagnetic ordering. This is also confirmed by field-cooled magnetization (Figure 7a) measurements. Below the minimum, a rapid increase in the $\chi_m T$ value (a great field dependence can be observed) occurs due to an increase of the ferromagnetic component of the weak ferromagnetic state. A maximum is observed at 30 K which is followed by swiftly decreasing moments until the lowest temperature of 2 K is reached due to saturation effects and or increasing antiferromagnetic correlations. This trend is also observed at higher fields but becomes less significant (in fact, it is nearly imperceptible at 10 000 G, Figure 6).

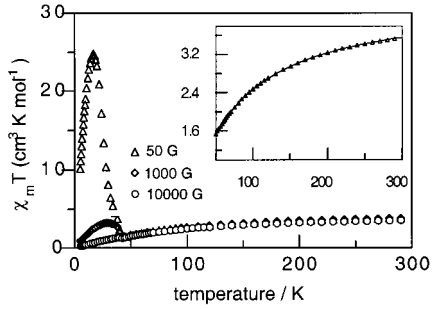

Figure 6. Thermal variation of $\chi_m T$ for **1** at different magnetic fields. The continuous line in the inset is the calculated curve.

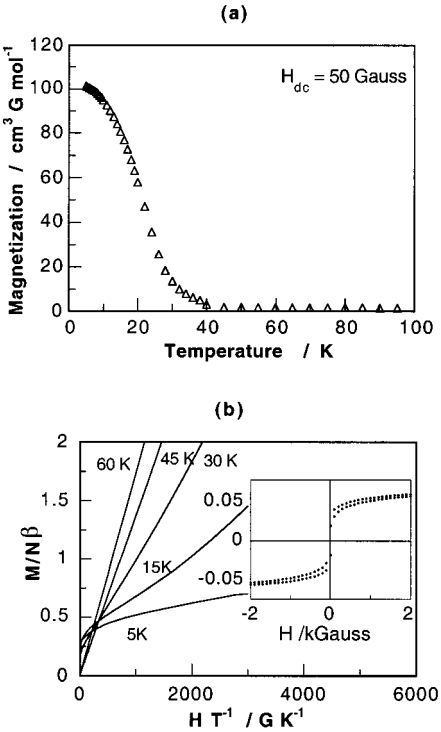

Figure 7. (a) Thermal variation of the molar magnetization for **1** ($H = 50$ G). (b) Magnetization vs H/T for **1** at several temperatures. The inset displays the hysteresis loop at 5 K.

(20) Carlin, R. L. *Magnetochemistry*; Springer: Berlin, 1986.
(21) Abragam, A.; Pryce, M. H. L. *Proc. R. Soc. London* **1951**, *A206*, 173.

For a weak ferromagnetism due to spin-canting, the magnetic behavior should be quite field dependent. Thus, with the aim of confirming the occurrence of spin-canting for **1**, magnetization values were measured at different temperatures and values of the applied field. The results indicate that, in the presence of small-applied dc fields, a spontaneous magnetization occurs for **1**. This is illustrated in Figure 7a where the thermal variation of the molar magnetization, M, at an applied field of 50 G is displayed. Thus, the abrupt increase of M below 45 K clearly indicates the occurrence of long-range magnetic ordering for **1**.

Further experimental evidence of the above-mentioned long-range magnetic ordering can be observed in Figure 7b where a set of M vs H/T curves is displayed. As observed, the linear curves corresponding to temperatures above 45 K agree with the occurrence of antiferromagnetic exchange coupling. The curves for $T < 45$ K, on the contrary, are linear just at high values of the magnetic field. It must be pointed out that in this temperature region the value of M at zero-field is different from zero, as corresponds to a ferromagnetic ground state. On the other hand, it is worth noticing that at $H < 2500$ G and $T < 45$ K magnetic hysteresis can be observed (inset in Figure 7b). A low saturation magnetization value consistent with weak ferromagnetic behavior is observed for **1**: $M = 750$ emu G mol^{-1} is reached at $H = 2000$ G, which is lower than the one expected for a system with $S = {}^5/_2$ ($M = 27925$ emu G mol^{-1}). This is consistent with the weak low-temperature ferromagnetism arising from the spin-canting below 45 K that has been proposed for **1**. The origin of the spin canting is proposed to be due to the presence of an antisymmetric term in the Mn−Mn exchange interaction.

To evaluate the antiferromagnetic interactions in a Heisenberg diamond-type network with $S = {}^5/_2$, HTS model can be used. In this case, even if the temperature range 50−300 K can be only analyzed, the fitting has been carried out in order to obtain approximate exchange values in the compound. The following equation[22] was used:

$$\chi = \frac{Ng^2\beta^2S(S+1)}{3kT}(1 + 23.3333x + 147.778x^2 + 405.487x^3 - 1621.13x^4 - 14201x^5 + 1037840x^6)(>)$$

where $x = J/kT$

This expression is based on the $H = -2J \sum_{\langle i,j \rangle} \hat{S}_i\hat{S}_j$ Hamiltonian. The best fit values, corresponding to the theoretical curve shown in the inset in Figure 6, are $J = -1.92$ cm^{-1} (-2.77 K) and $g = 2.00$ ($H = 50$ G, $T > 50$ K). As observed, excellent experiment-theory agreement is found.

The existence of low-temperature long-range magnetic ordering in compound **1** could also be observed in the heat-capacity measurements corresponding to this compound (Figure 8). Thus, it exhibits a peak at 40 K, associated to this ordering. Unfortunately, lattice contribution could not be estimated for the compound.

The magnetic data for compound **3** are displayed in Figure 9a as the thermal variation of χ_m^{-1} and χ_mT. As observed, the Curie−Weiss law is obeyed down to 130 K with values of C_m and θ of 2.95 cm^{3}Kmol^{-1} and -41.4 K. On the other hand, the χ_mT values slowly decrease from 2.61 cm^{3}Kmol^{-1}at 300 K to 2.09 cm^{3}Kmol^{-1} at ca. 75 K. Upon further cooling, the χ_mT value abruptly increases up to the temperature of 12 K and then finally decreases.

(22) Rushbrooke, G. S.; Wood, P. J. *Mol. Phys.* **1963**, *6*, 409.

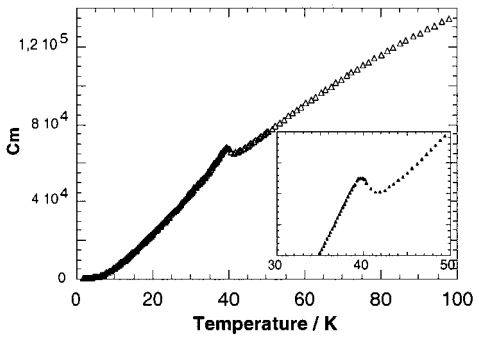

Figure 8. Heat-capacity measurements for [Mn(4,4′-bipy)(N_3)$_2$] (**1**).

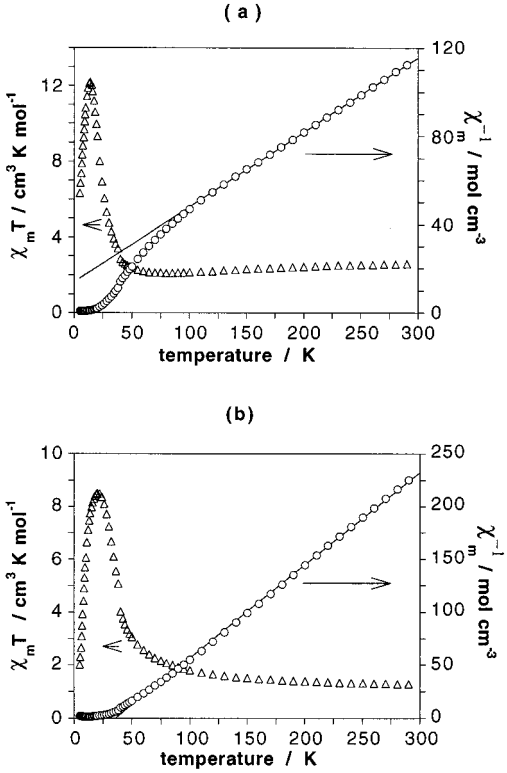

Figure 9. Thermal variation of χ_mT and χ_m^{-1} for (a) **3** and (b) **4**.

Measurements of the magnetic susceptibility were carried out also for **4**. Thus, as displayed in Figure 9b, the χ_m^{-1} magnitude follows the Curie−Weiss law down to 50 K with values of C_m and θ of 1.14 cm^3 K mol^{-1} and +35.6 K. The thermal variation of χ_mT, on the other hand, exhibits an increasing tendency for decreasing temperature that becomes very strong below 50 K. The curve reaches a maximum at 20 K and finally decreases tending to zero.

These results seem to indicate that a ferromagnetic component is taking place for **4**. This ferromagnetic character may be explained if considering the proposed azide dispositions in compounds **3** and **4**. Since the end-to-end azides and end-on ones with angles larger than 108° are known to transmit antiferromagnetic (AF) interactions, while end-on azido bridges transmit ferromagnetic (F) interactions, an −AF−AF−F− disposition similar to that shown in Scheme 1 could be possible for the metal ions, which would give rise to one uncoupled metal-spin for every three metal ions and therefore to ferromagnetic exchange in the compounds.

Since **3** and **4** are proposed to be isomorphous compounds, the above cited magnetostructural aspects may be also valid for **3.** Obviously, the distinct nature of the metallic cation must be considered in order to explain the differences observed

Scheme 1

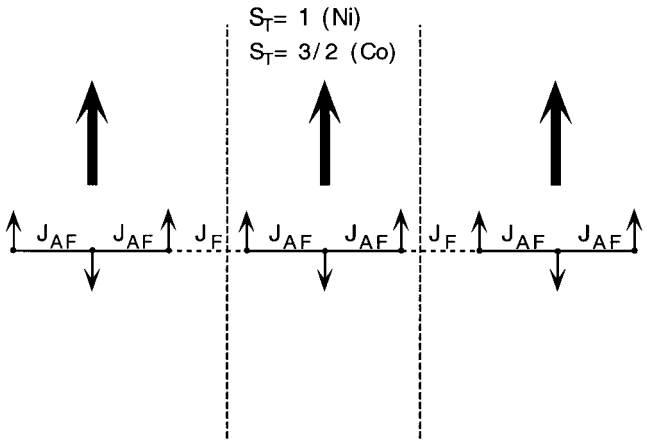

between **3** and **4** at high temperatures. In fact, the slow decrease of $\chi_m T$ at high temperatures exhibited by **3** corresponds to a single ion effect, characteristic of high-spin Co(II) that possesses an orbital momentum in the ground state. This results in a decrease of the $\chi_m T$ values in the high-temperature region that, in this particular case, is more significant than the expected increase due to the effective ferromagnetic coupling. The negative θ value in this compound must be associated to the spin−orbit coupling rather than to antiferromagnetic interactions.

Following the Scheme 1, ferrimagnetic-like chains could be expected for **3** and **4** even if the compounds are homometallic. Nevertheless, a typical ferrimagnetic behavior (decrease of $\chi_m T$ values down to a minimum and further increase) would only be observed when $J_{AF} \gg J_F$. On the contrary, if $J_F \gg J_{AF}$, an increase of $\chi_m T$ from room temperature up to a maximum, followed by a further decrease would be expected, the minimum appearing below 2K. The latter may be considered the situation for **3** and **4** since the ferromagnetic interactions through double-EO-azides are stronger than the corresponding antiferromagnetic ones through the mixed EE−EO azido-bridges.

In both **3** and **4** compounds, a ferromagnetic coupling of the resulting spins (Scheme 1) would finally led to $S_T = 1$ and $S_T = {}^3/_2$ spin states per Ni_3 and Co_3 units, respectively. Magnetization vs magnetic field measurements for both **3** and **4** compounds have been carried out (Figure 10) to test this hypothesis. Thus, saturation values of 0.66 e^- and 1 e^- per Ni and Co ions, respectively, have been obtained (Figure 10). These values agree with a $S = 1$ state per $[Ni_3(C_{10}H_8N_2)_3(N_3)_6]$ basic unit and a $S = {}^3/_2$ state per $[Co_3(C_{10}H_8N_2)_3(N_3)_6]$ basic unit, respectively, as proposed.

In the case of the Ni(II) compound **4**, a hysteresis loop can also be observed for fields below 10000 G, with M_r (remanent magnetization) and H_c (coercitive field) values of 204 emu G mol^{-1} and 1050 G, respectively (Figure 11).

Concluding Remarks

In this work, we report on the third known 3D coordination system exclusively based on azide links. This complex is, as the other previous two, a Mn(II) compound. However, the compound herein reported is acentric being constructed from symmetrical bridging units. From the experimental magnetic data for this compound, the presence of predominant antiferromagnetic coupling at high temperature, a phase transition at about 45 K, and the existence of a net magnetic moment at low temperature can be deduced. This information agrees with the existence of a long-range weak ferromagnetic coupling below the critical temperature, due to spin canting. The use of other M(II) cations, on the other hand, leads to a radically different structure which has been shown to be common for at least Zn(II), Co(II), and Ni(II). Magnetic measurements for **3** and **4** compounds show the existence of a ferromagnetic coupling of the spins with saturation magnetization values compatible with $S = 1$ and $S = {}^3/_2$ per Ni_3 and Co_3 units, respectively. Hysteresis is also observed for compound **4**.

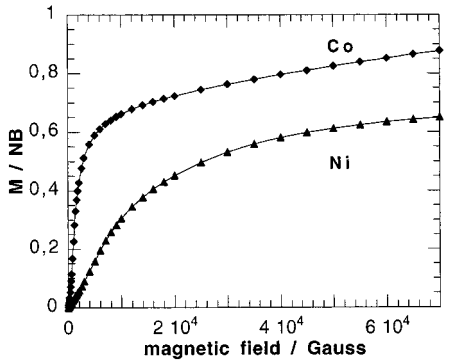

Figure 10. Magnetization vs H for **3** and **4** at the temperature of 5 K.

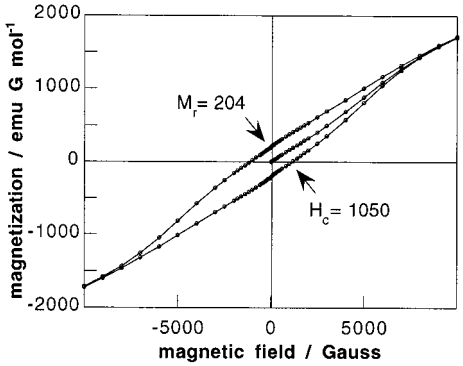

Figure 11. Hysteresis loop at 5 K for $[Ni(4,4'\text{-bipy})(N_3)_2]$ **4**.

Acknowledgment. This work has been carried out with the financial support of the Gobierno Vasco/Eusko Jaurlaritza (Project PI99/53) and the DGES PB97-0637 Grant. S.M. thanks the Gobierno Vasco/Eusko Jaurlaritza (Project PI96/39) for a doctoral fellowship.

Supporting Information Available: Listings of X-ray crystallographic data for compound **1** (CIF format) and powder diffraction data for **2**−**4**. This material is available free of charge via the Internet at http://pubs.acs.org.

IC001067Q